CRACK REPAIR OF STEEL VESSELS WITH BONDED COMPOSITE PATCHES – DAMAGE CONTROL WITH FBGS

E. Rodríguez[1*], R. de la Mano[1], L. Blanco[1]

[1]*Technology Center AIMEN, Relva 27A – Torneiros – Pontevedra – SPAIN*
**erodriguez@aimen.es*

Keywords: Repair, FBG, damage monitoring.

Abstract
One of the most important aspects regarding composites patch repairs in naval structures is the quality assurance of the damage repaired. In this paper crack monitoring procedure with optic Fibber Bragg Grating (FBG) strain sensors is described. Static and dynamic tests have been carried out to study the crack growth establishing strain differences between patched and un-patched structures. A progressive shift in strain distribution in the vicinity of the crack was observed. The experimental results demonstrated that a strain-based methodology can be utilized to detect crack propagation in this type of repairs.This project is being undertaken in the framework of a collaborative project (COPATCH) which is funded by the EC.

1 Introduction
Because of their properties, CFRP composites find application in many load bearing construction elements in aerospace, water and land transport, offshore and onshore pipelines, bridges and infrastructure applications. Nowadays, composites are also widely used for the repair of deteriorated and damaged structures. For example, the rehabilitation of bridges and buildings and the seismic retrofit of columns using composite reinforcements are widespread in the US, Canada, Europe and Japan [1,2]. The bonding offers excellent strength and fatigue properties due to the continuous nature of the connection. This arrangement gives a uniform stress distribution over the entire bonded area. Although the bonding technology is becoming increasingly popular, particularly in aircraft light alloys structures [3,4], this method of joining is still largely an unexplored idea in the shipbuilding industry, and the reported composite patch applications in steel marine structures are very few. Structural defects on ships, like cracks, are typically repaired by welding. However, welding has many disadvantages as the long operational time, hot-work, and shutdown of parts of the boat causing very expensive production delays or weight increases. Repairs with composite patch can be used as an alternative without any fire hazard and it is a lightweight solution. The patches are bonded over the defect and restore the integrity of the original structure [5,6]. Recently, the Project COPATCH [7] participated by a large consortium (including shipbuilders and a number of research bodies from 8 European nations) aims to establish this repair technique in the naval sector to demonstrate that composite patch repairs can be environmentally stable and therefore, that they can be used as long term repair measures. One of the most important aspects in this repair method is the crack growth control once the damage has been patched with CFRP composites. If the patch is applied to stop a crack in the steel, the crack tip and possible crack growth need to be monitored. In the present work, a

method for the in-situ monitoring of the crack propagation rate in the metallic plate repaired by a composite patch using optic Fibre Bragg Grating (FBG) strain sensors is described. A FBG is a few millimeters length microstructure that can be photo-inscribed in the core of a standard single mode telecom fibber. This pattern will induce a permanent change in the physical characteristics of the silica matrix. This change consists in a spatial periodic modulation of the core index of refraction that creates a resonant structure. When the fibber is stretched or compressed, it measures strain because the deformation of the optical fibber causes a change in the period of the microstructure and, consequently, of the Bragg wavelength. FBG sensors have been utilized to detect crack growth on aircraft panels [8,9] and, regarding the naval sector, have been incorporated in structural health monitoring of composite structures[10]. This work studies the suitability of FBG to monitor crack growth in naval steel repaired with composites.

2 Materials and experimental procedure

The steel plates used for manufacturing the testing specimens were normal grade A steel. The composite laminated patches were manufactured by hand lay-up with carbon fibber and vinylester resin. A full material characterization of the composites used for manufacturing the patches had been performed before initiation of the patched specimen tests. The main properties of both materials are summarized in Table 1.

Composite	***Properties***
Vinylester Resin (Reichhold)	Viscosity: 1000 mPa s
Carbon Fibber (Devold AMT)$[0]_2$	Density: 208 g/m^2 (each layer)
Composite (Hand Lay-up)	Modulus (tension$_{[0]}$): 74 GPa Maximum stress (tension$_{[0]}$): 1000 MPa w/w fibber: 50%

Steel	***Properties***
Naval Steel Grade A	Yield Strength: 315 MPa Max Tensile Strength: 455 MPa Elastic Modulus: 202 GPa

Table 1. Materials properties of composite patches and steel.

Steel plates had dimensions 200mm x 550mm x 5mm. Artificial cracks of 140mm and 50mm length were manufactured by EDM for static and fatigue tests respectively, and 0.3mm width both. The composite patch had thickness tp = 15mm, effective length Lp = 200mm and width Wp = 200mm. The total patch length was 300mm, since it additionally includes the tapered edges of the patch to avoid high debonding stresses at the patch edges.

Surface preparation of the steel before laminating the composite patches was carried out by two abrasives methods: sand blasting and needle gun. After that, the steel surface was degreased by isopropanol in order to remove rust, grease and oil. These methods obtained a quality SA2.5 but different roughness was achieved. The average surface roughness (Ra), and the root mean square average (Rq) of each specimen was measured in two directions, using a Dektak 8M - Veeco instrument in accordance with ISO 4288 standard. The specimens were installed into the hydraulic testing machine with the aid of specifically designed and manufactured fixtures as shows Figure 1. In the case of static tests, a preloading of 25 kN was first applied on the specimens, in order to minimize the specimen-fixtures assembly tolerances. The loading was then applied in the form of linearly increasing tensile displacement with a rate of 0.5 mm/s. In the case of fatigue test, different cycles were applied to the specimens with the objective of monitor the strain at the different loads from 10 to 250 kN, with an amplitude of 90 kN and a frequency of 0.1 s^{-1}. The tests end when the patch stops

contributing in the stiffness of the specimens and the steel enters into plasticity. Both static and fatigue test were carried out in a universal testing Hoytom machine with maximum load capacity of 600 kN.

Figure 1. A specimen on the hydraulic testing machine.

The curves of force versus total specimen elongation were recorded during each test. Strains at various locations of the specimens were monitoring with strain fiber optic sensors and strain gages to detect patch debonding and steel plasticity in locations close to the crack tip.
In static specimens, three strain gages (Kyowa, 5 mm length) were bonded, one on the top of the patch (named GC), in the center of the crack, and two in the back side at 100 mm of the crack tip (named GA and GB). Two strain FBGs (Fibersensing, 5 mm of grating) were also bonded on the back side at 100 mm from the crack tip but in the opposite side (FA and FB) to compare with strain gages values. In fatigue tests, only FBG were used. Two were bonded below the patch on the patch side at 15 mm from the crack tip (FA and FB) and one more on the back side at 5 mm from the crack tip (FC). The geometry of the specimens, crack positions and strain gages and FBGs positions are shown in Figure 2.

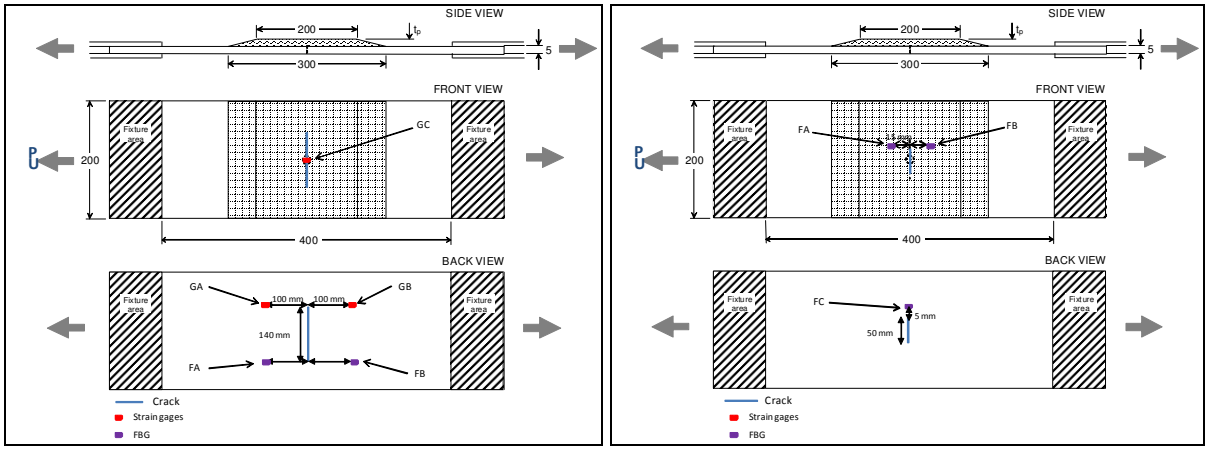

Figure 2. Dimensions of specimens and artificial crack positions. Left: Static test, Right: Fatigue test.

3 Results

3.1 Roughness measurements

The adhesive joint strength is seriously affected by the quality of the steel surface and there is a correlation between its roughness and the interactions with the adhesive layer of the composite in the patching process. For this reason, roughness has been measure in steel

treated with the two techniques. In Figure 3 the surfaces treated with sand blasting and needle gun are shown. It can be appreciated that sand blasting achieved a matt finish and fine grain. On the contrary, the surface of needle gun shows shiny and the grains are rounded. The measurements of roughness reflect these important differences between both treatments (Table 2). Sand blasting achieved Ra=10.6 μm and needle gun Ra=5.8 μm whereas the roughness of untreated steel is Ra= 0.5 μm. It is a clear effect of both treatments but sand blasting double the value of needle gun. There are not important deviations in 0º and 90º so the surface treatments have been properly carried out and preference directions were not produced.

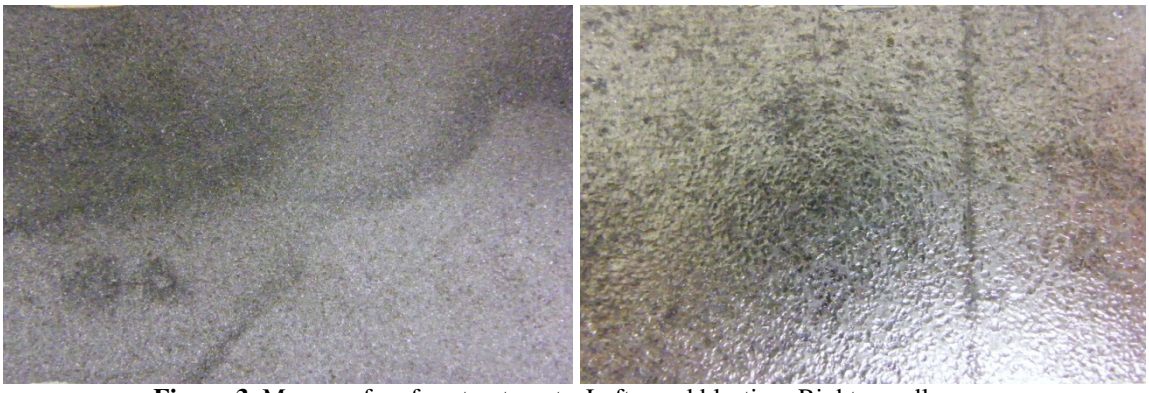

Figure 3. Macros of surface treatments. Left: sand blasting, Right: needle gun.

Sand Blasting	**Ra (μm)**	**Rq (μm)**	**Needle gun**	**Ra (μm)**	**Rq (μm)**
0º	10.6±0.4	13.4±0.3	0º	5.6±0.8	7.2±1.0
90º	10.6±0.5	13.7±0.7	90º	6.1±0.5	7.4±0.6
Average	10.6±0.4	13.6±0.5	Average	5.8±0.7	7.3±0.8
		Ra (μm)	**Rq (μm)**		
Steel (as received)		0.5±0.1	0.6±0.2		

Table 2. Average roughness of steel surfaces.

3.2 Results of static tests

Figure 4 is representative of the global behavior, showing the overall elongation as a function of the applied tensile load and Table 3 summarizes the failure values. The unpatched specimen exhibits a predictable behavior, with an initial linear elastic deformation to 76.5 kN, followed by entrance into plasticity to a maximum load value of 134 kN and finally crack opening occurs. These values match the theoretically calculated value using simple formulae of mechanics. Similar behavior has the patched-needle gun specimen which reflects a maximum load of 131.5 kN. However, the linear elastic response region of the patched-sand blasting is much bigger than the corresponding one of the unpatched specimen. This can be explained by the fact that, due to the presence of the patch, the steel substrate is loaded by lower stresses for the same applied load, thus it behaves elastically up to higher applied loads. In the sequence, failure of bonding between the patch and the steel plate is taking place at 258.5 kN, resulting in a sudden drop of the load carried by the specimen, since the patch is no longer carrying load and the plasticity of the steel occurs in this point as unpatched specimen.

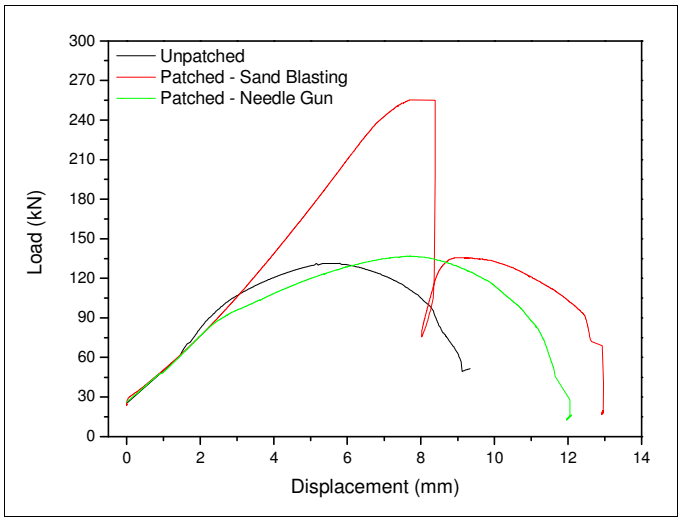

Figure 4. Elongation *vs* applied load.

	Yield (kN)	Max. Load (kN)
Unpatched	76.5 ± 1.5	134.0 ± 3.0
Patched – Sand blasting	-	258.5 ± 3.5
Patched – Needle gun	-	131.5 ± 4.5

Table 3. Failure load of specimens.

It is a clear difference between patched samples depending on surface treatments. Needle gun acts as unpatched sample because there is not good adhesion of the composite patch with steel. The patch debonded when the steel overcome the elastic limit derived in an adhesive failure. It means that the resin of the adhesive layer was not properly bonded to the steel and the patch did not retain the crack opening. On the contrary, sand blasting shows the best result with cohesive failure zones as shows Figure 5. Fragments of composite remain in the steel surface which means that a good interaction resin-steel has occurred. The effectiveness of the composite patch is affected by the quality of the adhesive layer and it depends on the surface preparation. The higher strength of the joint composite-sand blasting surface is related with its higher roughness, sand blasting achieved Ra=10.6 μm and needle gun Ra=5.8 μm, and higher roughness means more surface for joining so more bonding strength.

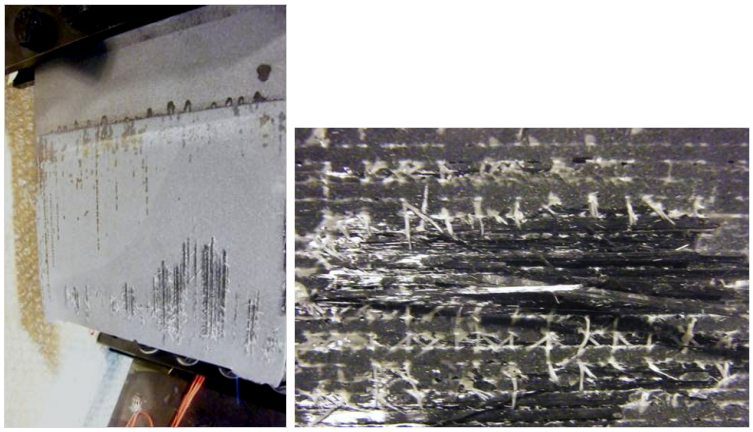

Figure 5. Left: Steel sand blasting surface after patch failure. Right: composite patch delaminated fragments

Regarding strain measurements, Figure 6 shows the values obtained by gages and FBGs, situated in the locations explained in the Figure 2**,** during the static tests. Only sand blasting specimen in explained because of the best result obtained with this treatment. In the

unpatched specimen the strain values in A and B increase when the load increases. The behavior of load and strain curves is the same during elastic region and when the plasticity of the specimen occurs with a non-linear increment. Once the maximum load is achieved and the crack began opening the strain in crack tips decrease as represent both A and B FBGs curves. In the A and B gages curves this drop occurs later because the side of the crack which first opened was where FBG were bonded. The same behavior found between FBGs and gages shows the properly running of the new system proposed to crack monitoring. In the patched specimen we can see also this fact; A and B FBGs and gage curves have the same behavior that load in the back side of the specimen. The strain increases and it means that tensile stresses are acting on crack tip in this side, but, on the contrary, the gage sited on the top of the patch (gage C) shows completely different behavior. When the load increases strain decreases, in other words, a compression force results on the patch. This explains the effectiveness of the patch slowing down the crack growth because the adhesive layer is transferring forces from the crack tips to the composite causing a similar effect of bending on the global specimen. In preceding load of the maximum value, the strain shows an increment still final debonded failure when relaxation of the patch occurs and gage C did not exhibit strain. The strain on back side achieved maximum values at maximum loads while the crack is hold and when the patch failure occurs the crack tips show plasticity and crack opening registered by gages and FBGs. Table 4 shows strain values achieved on both types of specimen. The effect of the patch holding the crack is reporting by gages and FBGs that show similar values at yield point (~300με) and after that strain in patched specimen is increasing on tip cracks until patch failure (~1000με).

		Strain in yield (με)		Strain in max.load** (με)	
Specimen	**Sensor**	**A**	**B**	**A**	**B**
Unpatched	Gage	300	300	800	870
	FBG	300	320	800	870
Patched sand blasting	Gage	280	310	1000	1000
	FBG	300	250	900	1050

* Strain when the specimen achieves the yield point (76 kN)
** Strain at the maximum load for each specimen (unpatched: 134 kN and patched: 258 kN)

Table 4. Strain values in unpatched and patched specimens at different points of the static test.

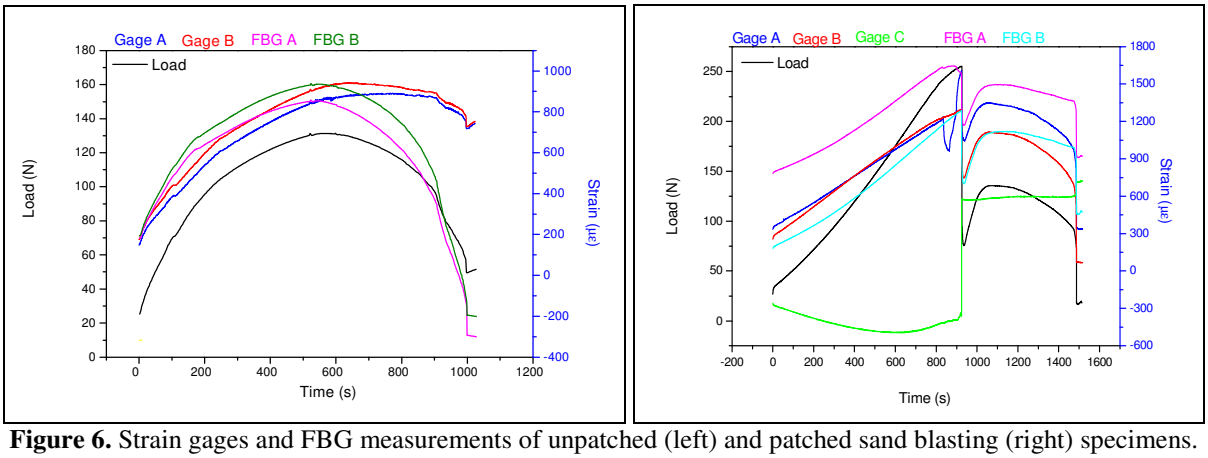

Figure 6. Strain gages and FBG measurements of unpatched (left) and patched sand blasting (right) specimens.

3.3 Results of fatigue tests

The main objective of this test was to analyse the capability of FBGs to monitor patch debonding and crack opening. In the Figure 7 the cycles applied in a patched sand blasting specimen are shown. Increasing loading cycles show increasing strains, but at 310 kN the fixtures failure occurs before patch debonding. The most important information that can be

extracted from this test is the difference between strains below the patch (A and B) which are much lower than strains in steel side due to the effect of the composite patch. On the contrary, in a specimen patched-needle gun (Figure 8) the strains are similar in positions A, B and C upt to 110 kN when patch debonding begin.

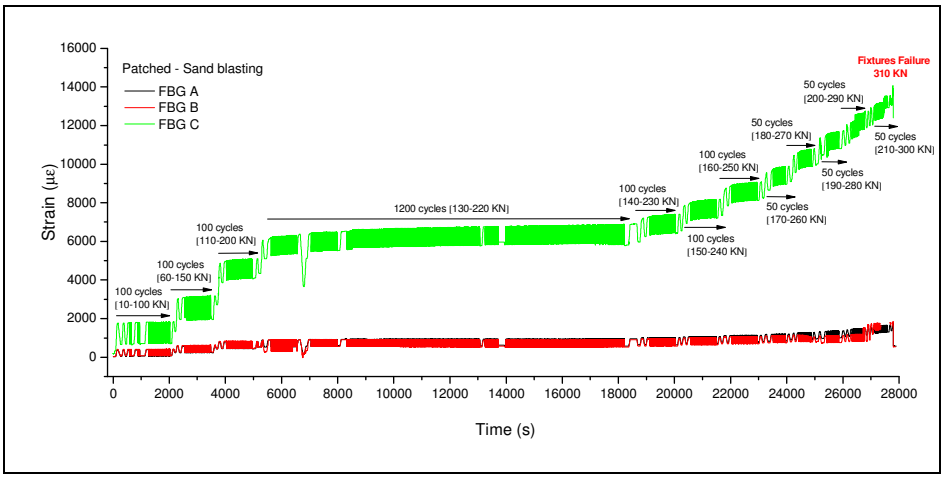

Figure 7. Strain values of FBGs during fatigue cycles of a patched-sand blasting.

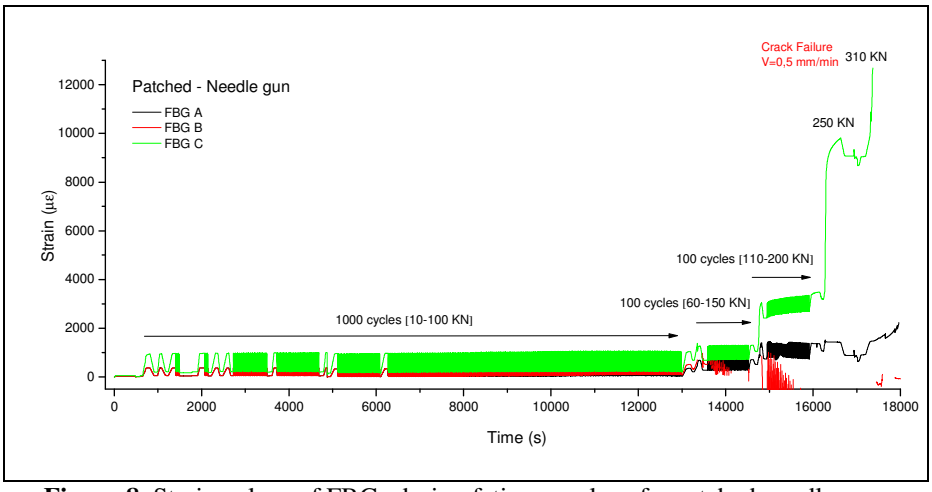

Figure 8. Strain values of FBGs during fatigue cycles of a patched-needle gun.

There is evidence that the patch in this case is not holding the crack. The crack opening occurs at 310 kN and the signals of FBGs were lost at this tensile load. In the Figure 9 the values of strain at the same loads and cycles are represented for unpatched and needle gun-patched.

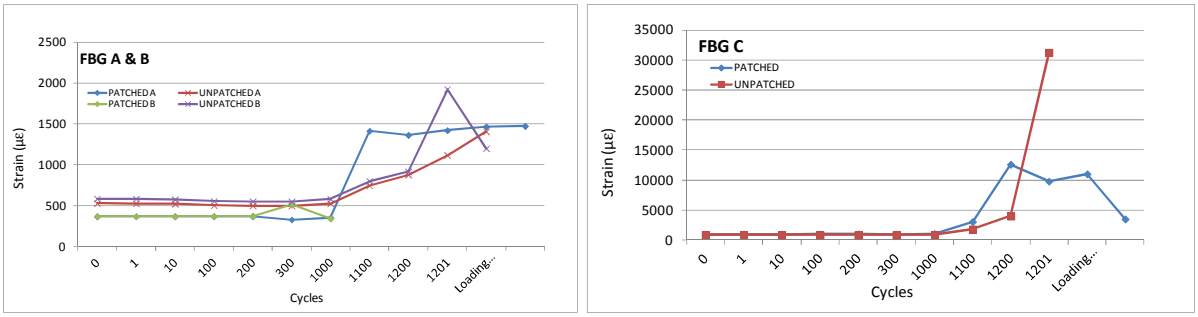

Figure 9. Comparative graphs of strains in fatigue tests of patched-needle gun and unpatched specimens

In positions A and B of unpatched specimens strains are higher and the increase can be seen when plasticity and crack opening occurs (1000 cycles). In the case of patched specimen at this number of cycles patch debonding occurs and a sudden increase of strain on the crack tip is recorded. In FBG C (back side) strain in both specimens is similar but when patch failure starts the strain in unpatched specimen is higher.

4 Conclusions

The experimental study carried out resulted in the following conclusions:
- The maximum load achieved in patched specimens doubles the unpatched values.
- Sand blasting achieved a surface roughness that improves the adhesion between steel and composite.
- Specimens responded linearly elastically until debonding and arresting the crack. After this, all specimens followed the typical steel behaviour, being deformed plastically.
- FBGs have shows its capability to monitor the patch debonding and crack opening.

Acknowledges

The research leading to these results has received funding from the European Union's Seventh Framework Programme (FP7/2007-1013) under grant agreement No. 233969.

References

[1] Roberts J.E. *Application of composites in California bridges* in "Proceedings of *Composites in the Transportation Industry (ACUN-2)*", Sydney, Australia, **1**, pp 1–15 (2000).
[2] Karbhari V.M. *FRP composites for infrastructure renewal-status and challenges for the 21st century* in: "Proceedings of *Composites in the Transportation Industry (ACUN-2)*", Sydney, Australia, **1**, pp 51–60 (2000)
[3] A. Chukwujekwu, Navdeep Singh, U.E. Enemuoh, S.V. Rao. Design, analysis and performance of adhesively bonded composite patch repair of cracked aluminum aircraft panels. *Composite Structures,* **71,** pp 258–270 (2005).
[4] Dae-Cheol Seo, Jung-Ju Lee. Fatigue crack growth behavior of cracked aluminum plate repaired with composite patch. *Composite Structures*, **57**, 323–330 (2002).
[5] T.J. Turtona, J. Dalzel-Jobb, F. Livingstone. Oil platforms, destroyers and frigates—case studies of QinetiQ's marine composite patch repairs. *Composites: Part A*, **36**, 1066–1072 (2005).
[6] J Dalzel-Job. Composite patch repair of steel ships. *Advanced Marine Materials: Technology & Applications Conference,* London, UK (2003).
[7] www.co-patch.com
[8] Gifford DK, et al. Structural integrity monitoring of aircraft panels using a distributed Bragg grating sensing technique. *Smart structures and materials 2003*. Smart Sensor Technol Measure Syst, **5050**, pp 358–66 (2003).
[9] Li S, Wu Z. Development of distributed long-gage fiber optic sensing system for structural health monitoring. *Struct Health Monitor*, **6(2)**, pp133–43 (2007).
[10] Okabe Y, Yashiro S, Kosaka T, Takeda N. Detection of transverse cracks in CFRP composites using embedded Bragg grating sensors. *Smart Mater Struct* **9(6)** 832–8 (2000).